Ruthenium Derivatives of NiS_2N_2 Complexes as Analogues of Bioorganometallic Reaction Centers

Michael A. Reynolds, Thomas B. Rauchfuss,* and Scott R. Wilson

Department of Chemistry, University of Illinois at Urbana−Champaign, 600 S. Mathews Avenue, Urbana, Illinois 61801

Received September 3, 2002

Recent results from structural biology demonstrate the catalytic significance of $Ni(SR)_2L_2$ centers attached to a second metal that binds CO, in particular the NiFe hydrogenases and acetyl CoA synthase. In experiments aimed at developing bimetallic derivatives exhibiting an affinity for CO, we have studied Ru(II) derivatives of nickel diaminodithiolates and the reactivity of these complexes toward CO and other small molecules. The reaction of $[Cp^*Ru(NCMe)_3]OTf$ and NiS_2N_2 (S_2N_2 = *N*,*N*′-bis(2-mercaptoethyl)-*N*,*N*′-dimethyl-1,3-diaminoethane) gives $[Cp^*Ru(NiS_2N_2)]_2(OTf)_2$ ($[\mathbf{1}]_2(OTf)_2$), which exists as a monomer−dimer equilibrium in MeCN solution. Crystallographic analysis of $[\mathbf{1}]_2(OTf)_2$ reveals a centrosymmetric dication with the Ru being quasi-octahedral and the NiS_2N_2 coordination sphere being relatively planar, the metal centers being linked via pairs of μ_2-SR and μ_3-SR units. Complex $[\mathbf{1}]_2^{2+}$ oxygenates and sulfidizes with O_2 and S_8, respectively, to give $[Cp^*Ru(NiS_2N_2)(\eta^2\text{-}E_2)]^+$ (E = O, S), which were characterized spectroscopically and crystallographically. Solutions of $[\mathbf{1}]_2(OTf)_2$ also react with CO and MeNC to give the corresponding adducts $[Cp^*Ru(NiS_2N_2)L]OTf$, where L = CO and MeNC. The ν_{CO} = 1901 cm^{-1} for the CO adduct indicates the excellent donating power of the NiS_2N_2 ligand. The Cp^*Ru^+ derivative of the bulkier version of the NiS_2N_2 species, Ni(bme*-daco) (bme*-daco = [1,5-bis(2-mercapto-2-methylpropyl)-1,5-diazacyclooctane]), is the monomeric analogue of $\mathbf{1}^+$, $[Cp^*Ru(NCMe)(Ni(bme^*\text{-}daco))]^+$, whose structure was confirmed spectroscopically and crystallographically. In this species the thiolato ligands are doubly bridging and the Cp*Ru subunit adopts the usual piano-stool geometry with a terminal MeCN ligand. The MeCN is readily displaced by CO and O_2 to give the corresponding adducts. The reaction of $CpRu(PPh_3)_2Cl$ and NiS_2N_2 produced the PPh_3 adduct $[CpRu(NiS_2N_2)(PPh_3)]Cl$, wherein the PPh_3 ligand is nonlabile. The corresponding reaction of NiS_2N_2 with sources of $(arene)RuCl^+$ gave the expected adducts $[(arene)Ru(Cl)(NiS_2N_2)]^+$, isolated as their OTf^- salts.

Introduction

Nature employs hydrogenase enzymes for the sensing and conversions of dihydrogen. These enzymes can be classified according to the metal content at their active sites: Fe-only, NiFe, and metal free.[1] The active sites of all three enzyme classes exhibit remarkably novel structures, especially in the organometallic context. A mechanistic understanding of these enzymes would be significant for both basic organometallic chemistry as well as the commercial utilization of dihydrogen. In the case of the Fe-only hydrogenases, low molecular weight models have achieved at least a rudimentary level of success with respect to structure[2,3] and function.[4]

Despite the fact that high-resolution crystal structures of the enzyme have been available for several years,[5−7] little progress has been achieved in the characterization of Ni-Fe complexes with suitable reactivity. The active sites of the NiFe enzymes consist of a dithiolate-linked Ni-Fe center that bears little resemblance to known compounds (Chart 1). Furthermore, the exact site of H_2 activation remains controversial.[8−11] One reason to expect H_2 binding at Fe is the wealth of precedent for ferrous H_2 complexes.[12−16]

Chart 1. Active Site Structures for Acetyl CoA Synthase (ACS) and NiFe Hydrogenase

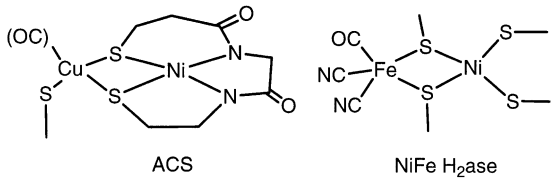

(1) Thauer, R. K.; Klein, A. R.; Hartmann, G. C. *Chem. Rev.* **1996**, *96*, 3031−3042.
(2) Gloaguen, F.; Lawrence, J. D.; Schmidt, M.; Wilson, S. R.; Rauchfuss, T. B. *J. Am. Chem. Soc.* **2001**, *123*, 12518−12527.
(3) Lawrence, J. D.; Rauchfuss, T. B.; Wilson, S. R. *Inorg. Chem.* **2002**, *41*, 6193−6195.
(4) Gloaguen, F.; Lawrence, J. D.; Rauchfuss, T. B. *J. Am. Chem. Soc.* **2001**, *123*, 9476−9477.
(5) Marr, A. C.; Spencer, D. J. E.; Schroder, M. *Coord. Chem. Rev.* **2001**, *219*−*221*, 1055−1074.
(6) Forde, C. E.; Morris, R. H. *Electron Transfer Chem.* **2001**, *2*, 905−926.
(7) Frey, M. *ChemBioChem* **2002**, *3*, 153−160.
(8) Pavlov, M.; Siegbahn, P. E. M.; Blomberg, M. R. A.; Crabtree, R. H. *J. Am. Chem. Soc.* **1998**, *120*, 548−555.
(9) Amara, P.; Volbeda, A.; Carlos, J. C.; Fontecilla-Camps, J. C.; Field, M. J. *J. Am. Chem. Soc.* **1999**, *121*, 4468−4477.
(10) Niu, S.; Thomson, L. M.; Hall, M. B. *J. Am. Chem. Soc.* **1999**, *121*, 4000−4007.

10.1021/om020724e CCC: $25.00
Publication on Web 03/14/2003

Chart 2. Structural Models for the Ni-Fe Hydrogenase Metalloenzyme Active Site[a]

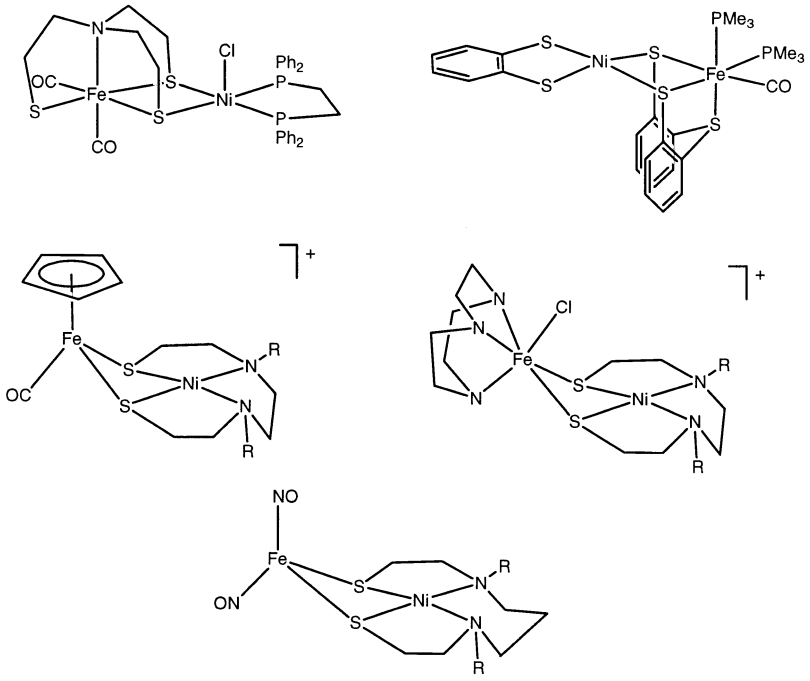

[a] See text for references.

Representative synthetic models for the NiFe-hydrogenase active site are shown in Chart 2. The primary focus has been on the preparation of the Ni(μ-SR)$_2$Fe centers, which are observed in the enzyme structure. Commonly such bimetallic complexes are prepared by the interaction of iron reagents with diaminodithiolates of Ni(II). These diaminodithiolate building blocks comprise a fairly large class of complexes.[17] The Ni(SR)$_2$(NR$_3$)$_2$ coordination set simulates the Ni(SR)$_4$ site seen crystallographically in the enzymes.[18−21] Two unresolved deficiencies with the applicability of Ni(SR)$_2$(NR$_3$)$_2$ as a subunit in these models are (i) that the naturally occurring nickel thiolate is distorted toward the tetrahedral geometry, whereas the nickel is typically planar in its diaminodithiolates, and (ii) the naturally occurring Ni(SR)$_4$ site is probably anionic. The other half of the bimetallic active site features an Fe(CN)$_2$(CO) subunit, as established by combined crystallographic and spectroscopic studies. Many examples of Fe-CN-CO species have been examined recently,[22−24] some even linked to a nickel thiolate.[25] Bimetallic derivatives of Ni(SR)$_2$(NR$_3$)$_2$ complexes are also relevant to the recently characterized active site of acetyl CoA synthase (ACS, Chart 1), which features a diamido-dithiolato nickel center linked to copper via two thiolato bridges. ACS is responsible for forming acetyl groups, which may occur via methyl transfer from nickel to a Cu-bound CO ligand.[26]

Several years ago we started to explore the synthesis of *fac*-L$_3$Fe(II) complexes of the NiS$_2$N$_2$ in a search for complexes that would exhibit some reactivity at one of the two metals. Initial studies focused on (Me$_3$TACN)-Fe^{2+} derivatives (Me$_3$TACN = *N*,*N*′,*N*″-trimethyltriazacyclononane). We synthesized the species [(Me$_3$TACN)-FeCl(NiS$_2$N$_2$)]$^+$ via the reaction of (Me$_3$TACN)FeCl$_2$ [27] with standard Ni(SR)$_2$(NR$_3$)$_2$ building blocks, but the resulting bimetallic complex, which was high spin, showed little affinity for π-acid ligands.[28] In a revised approach, we synthesized the low-spin complex [CpFe-(CO)(NiS$_2$N$_2$)]$^+$ via the reaction of [CpFe(CO)$_2$(CH$_2$-CMe$_2$)]BF$_4$ again using the NiS$_2$N$_2$ building block. The resulting salt {CpFe(CO)[NiS$_2$N$_2$]}BF$_4$, also characterized crystallographically,[29] was found to be substitutionally inert. The lack of suitable reactivity in these Ni-Fe species led us to redirect our efforts toward Ru analogues with the knowledge that Ru(II) typically exhibits a high affinity for π-acid ligands and H$_2$.[30] In this paper

(11) Stein, M.; Lubitz, W. *Curr. Opin. Chem. Biol.* **2002**, *6*, 243−249.
(12) Scharrer, E.; Chang, S.; Brookhart, M. *Organometallics* **1995**, *14*, 5686−5694.
(13) Morris, R. H.; Sawyer, J. F.; Shiralian, M.; Zubkowski, J. *J. Am. Chem. Soc.* **1985**, *107*, 5581−5582.
(14) Amrhein, P. I.; Drouin, S. D.; Forde, C. E.; Lough, A. J.; Morris, R. H. *J. Chem. Soc., Chem. Commun.* **1996**, 1665−1666.
(15) Landau, S. E.; Morris, R. H.; Lough, A. J. *Inorg. Chem.* **1999**, *38*, 6060−6068.
(16) Kubas, G. J. *Metal Dihydrogen and σ-Bond Complexes*; Kluwer Academic/Plenum Publishers: New York, 2001.
(17) Krüger, H.-J.; Peng, G.; Holm, R. H. *Inorg. Chem.* **1991**, *30*.
(18) Volbeda, A.; Charan, M.-H.; Piras, C.; Hatchikian, E. C.; Frey, M.; Fontecilla-Camps, J. C. *Nature* **1995**, *373*, 580−587.
(19) Volbeda, A.; Garcin, E.; Piras, C.; de Lacey, A. L.; Fernandez, V. M.; Hatchikian, E. C.; Frey, M.; Fontecilla-Camps, J. C. *J. Am. Chem. Soc.* **1996**, *118*, 12989−12996.
(20) Garcin, E.; Vernede, X.; Hatchikian, E. C.; Volbeda, A.; Frey, M.; Fontecilla-Camps, J. C. *Structure* **1999**, *7*, 557−566.
(21) Higuchi, Y.; Ogata, H.; Miki, K.; Yasuoka, N.; Yagi, T. *Structure* **1999**, *7*, 549−556.
(22) Lai, C.-H.; Reibenspies, J. H.; Darensbourg, M. Y. *Angew. Chem., Int. Ed. Engl.* **1996**, *35*, 2390−2393.
(23) Rauchfuss, T. B.; Contakes, S. M.; Hsu, S. C. N.; Reynolds, M. A.; Wilson, S. R. *J. Am. Chem. Soc.* **2001**, *123*, 6933−6934.
(24) Sellmann, D.; Geipel, F.; Heinemann, F. W. *Chem. Eur. J.* **2002**, *8*, 958−966.
(25) Sellmann, D.; Geipel, F.; Lauderbach, F.; Heinemann, F. W. *Angew. Chem., Int. Ed.* **2002**, *41*, 632−634.
(26) Doukov, T. I.; Iverson, T. M.; Seravalli, J.; Ragsdale, S. W.; Drennan, C. L. *Science* **2002**, *298*, 567−572.
(27) Moreland, A. C.; Rauchfuss, T. B. *Inorg. Chem.* **2000**, *39*, 3029−3036.
(28) Moreland, A. C. Unpublished results, 2000.
(29) Eckermann, A. L., Ph.D. Thesis, University of Illinois at Urbana-Champaign, 2003.

Chart 3. Structures of NiS_2N_2 and Ni(bme*-daco) Metalloligands[a]

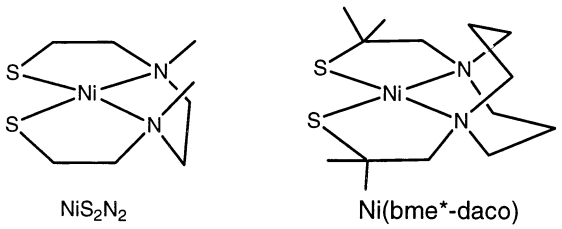

[a] See text for references.

we summarize these results, focusing especially on $(C_5R_5)Ru^+$ and $(C_6R_6)Ru^{2+}$ derivatives of the NiS_2N_2 metalloligands. We demonstrate that the Ru center, used as a surrogate for the naturally occurring Fe, is reactive toward π-acid ligands.

Results and Discussion

The overall synthetic methodology followed in this work entails treatment of various ruthenium electrophiles with nickel complexes of either of two diamino dithiolates, which are shown in Chart 3.

Synthesis of $[Cp^*Ru(NiS_2N_2)]_2(OTf)_2$ ($[\mathbf{1}]_2(OTf)_2$). Treatment of MeCN solutions of $[Cp^*Ru(MeCN)_3]OTf$ with NiS_2N_2 furnished dark brown $[Cp^*Ru(NiS_2N_2)]_2(OTf)_2$ ($[\mathbf{1}]_2(OTf)_2$) in excellent yield (eq 1).

$$2\ [Cp^*Ru(NCMe)_3]OTf + 2\ NiS_2N_2 \xrightarrow{-6\ MeCN} [Cp^*Ru(NiS_2N_2)]_2(OTf)_2 \quad (1)$$
$$[\mathbf{1}]_2(OTf)_2$$

The salt $[\mathbf{1}]_2(OTf)_2$ is moderately air-stable in the solid state but rapidly oxygenates when exposed to air in solution (see below). ^1H NMR spectroscopic analysis of $[\mathbf{1}]_2(OTf)_2$ in CD_3CN showed broadened signals that were shifted downfield of those in the free NiS_2N_2. Upon cooling the solution to −30 °C, two subspectra can be resolved, which we attribute to $[Cp^*Ru(NiS_2N_2)(CD_3CN)]^+$ and $[Cp^*Ru(NiS_2N_2)]_2^{2+}$ (eq 2).

$$[Cp^*Ru(NiS_2N_2)]_2^{2+} + 2\ MeCN \rightleftharpoons 2\ [Cp^*Ru(NiS_2N_2)(MeCN)]^+ \quad (2)$$
$$[\mathbf{1}]_2^{2+}$$

The high-temperature ^1H NMR spectrum is simple, due to rapid monomer−dimer equilibria, with the equilibrium favoring the monomer $[Cp^*Ru(NiS_2N_2)(NCMe)]^+$ (Supporting Information). The ESI-MS spectrum of $[\mathbf{1}]_2(OTf)_2$ shows a parent ion with $m/z = 501$ corresponding to $Cp^*Ru(NiS_2N_2)^+$, i.e., one-half of the dimer unit. Signals for $[Cp^*Ru(NiS_2N_2)(NCMe)]^+$ were not observed.

Crystallographic analysis of $[\mathbf{1}]_2(OTf)_2$ reveals a centrosymmetric dication with the Ru centers being quasi-octahedral and the NiS_2N_2 coordination sphere being relatively planar (Figure 1, Table 1). The Ru and Ni centers are linked via the two μ-SR units. All three Ru−S distances fall in a narrow range of 2.4736(16)−2.4396(17) Å. The Ni environment of the NiS_2N_2 moiety is similar to that observed in $[Ni(NiS_2N_2)_2]^{2+}$.[31]

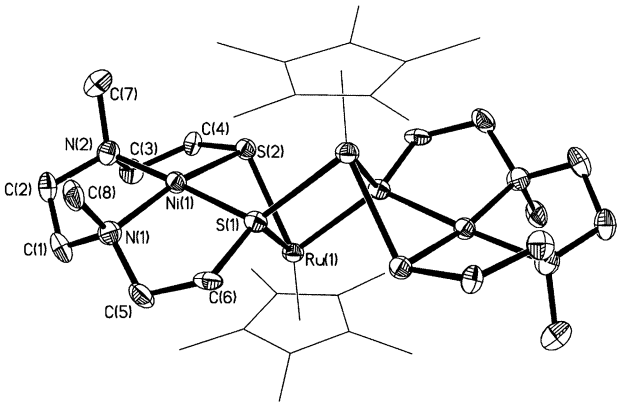

Figure 1. Molecular structure of the dication in $[Cp^*Ru(NiS_2N_2)]_2(OTf)_2$, $[\mathbf{1}]_2(OTf)_2$, with thermal ellipsoids drawn at the 50% probability level.

Table 1. Selected Bond Lengths (Å) and Angles (deg) for $[\mathbf{1}]_2(OTf)_2$

Ru(1)−S(1)	2.4736(16)	S(1)−Ru(1)−S(1A)	73.81(7)
Ru(1)−S(2)	2.4672(17)	S(2)−Ru(1)−S(1A)	81.61(6)
Ru(1)−S(1A)	2.4396(17)	S(1)−Ni(1)−S(2)	88.15(7)
Ni(1)−S(1)	2.1401(18)	N(1)−Ni(1)−N(2)	88.6(2)
Ni(1)−S(2)	2.1761(17)	C(6)−S(1)−Ru(1)	122.1(2)
Ni(1)−N(1)	1.938(5)	C(6)−S(1)−Ni(1)	98.9(2)
Ni(1)−N(2)	1.943(5)	Ru(1)−S(1)−Ni(1)	83.41(5)
S(1)−Ru(1)−S(2)	74.84(5)	Ru(1A)−S(1)−Ni(1)	124.10(7)

Complex $[\mathbf{1}]_2^{2+}$ proved to be unreactive toward PhCCH, cyclohexene, Et_3SiH, H_2O, protic acids, and H_2 in both MeCN and $MeNO_2$, although it does react with O_2, S_8, CO, and CNMe as described below. Reactions of $[\mathbf{1}]_2^{2+}$ with more aggressive reagents such as $LiAlH_4$, $NaBH_4$, and NaOMe led to decomposition into NiS_2N_2 and unidentified ruthenium-containing products. Reaction of $[Cp^*RuCl]_4$ with 4 equiv of NiS_2N_2 in MeCN produced the chloride salt of $[\mathbf{1}]_2^{2+}$, as indicated by ^1H NMR spectroscopy.

Reactivity of $[\mathbf{1}]_2(OTf)_2$ with O_2 and S_8. Exposure of an MeCN solution of $[\mathbf{1}]_2(OTf)_2$ to air quantitatively afforded the red-brown peroxo species $[Cp^*Ru(NiS_2N_2)(\eta^2\text{-}O_2)]OTf$ ($[\mathbf{2}]OTf$) (eq 3).

$$[Cp^*Ru(NiS_2N_2)]_2^{2+} + 2\ O_2 \rightarrow 2\ [Cp^*Ru(NiS_2N_2)(O_2)]^+ \quad (3)$$
$$[\mathbf{1}]_2^{2+} \qquad \mathbf{2}^+$$

ESI-MS analysis confirms the formula ($m/z = 533.1$). Aside from the methylene signals, the ^1H NMR spectrum shows a singlet for the two NMe groups and a singlet for Cp* shifted 0.12 ppm upfield vs $[\mathbf{1}]_2^{2+}$. Crystallographic analysis confirms the close similarity of the Ru-Ni bimetallic unit in $\mathbf{2}^+$ and $[\mathbf{1}]_2^{2+}$ (Figure 2, Table 2). In principle, the species $[Cp^*Ru(L)(NiS_2N_2)]$ could exist as four possible isomers; however only one isomer (Chart 4) was observed for $\mathbf{2}^+$. In terms of the relative stereochemistry, the Cp* ligands in $[\mathbf{1}]_2^{2+}$ are axial, while the Cp* in $\mathbf{2}^+$ is equatorial. Cations $[Ni(NiS_2N_2)]_2^{2+}$ and $Fe(NO)_2[Ni(S_2N_2')]$ ($S_2N_2' = N,N'$-

(30) Law, J. K.; Mellows, H.; Heinekey, D. M. *J. Am. Chem. Soc.* **2002**, *124*, 1024−1030.

(31) Turner, M. A.; Driessen, W. L.; Reedijk, J. *Inorg. Chem.* **1990**, *29*, 3331−3335.

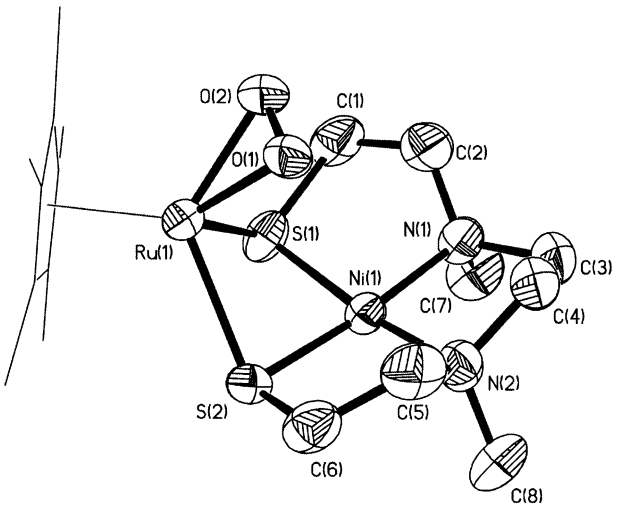

Figure 2. Molecular structure of the cation of [Cp*Ru(NiN_2S_2)(η^2-O_2)](OTf), [**2**](OTf), with thermal ellipsoids drawn at the 30% probability level.

Table 2. Selected Bond Lengths (Å) and Angles (deg) for [2]OTf

Ru(1)−O(1)	2.054(6)	O(2)−Ru(1)−S(1)	86.1(3)
Ru(1)−O(2)	2.041(6)	S(1)−Ni(1)−S(2)	87.74(8)
Ru(1)−S(1)	2.418(2)	N(1)−Ni(1)−N(2)	89.3(2)
Ru(1)−S(2)	2.4086(19)	N(1)−Ni(1)−S(1)	90.45(16)
O(1)−O(2)	1.371(8)	N(2)−Ni(1)−S(2)	90.75(17)
Ni(1)−S(1)	2.144(2)	C(1)−S(1)−Ru(1)	111.8(3)
Ni(1)−S(2)	2.130(2)	C(1)−S(1)−Ni(1)	96.8(3)
Ni(1)−N(1)	1.939(5)	Ru(1)−S(1)−Ni(1)	82.84(7)
Ni(1)−N(2)	1.925(5)	C(6)−S(2)−Ru(1)	114.0(3)
O(1)−Ru(1)−O(2)	39.1(2)	Ni(1)−S(2)−Ru(1)	83.36(6)
S(1)−Ru(1)−S(2)	75.71(7)	C(6)−S(2)−Ni(1)	98.5(3)
O(1)−Ru(1)−S(2)	95.6(3)		

Chart 4. Possible Isomers of [Cp*Ru(L)(NiS_2N_2)]$^{+a}$

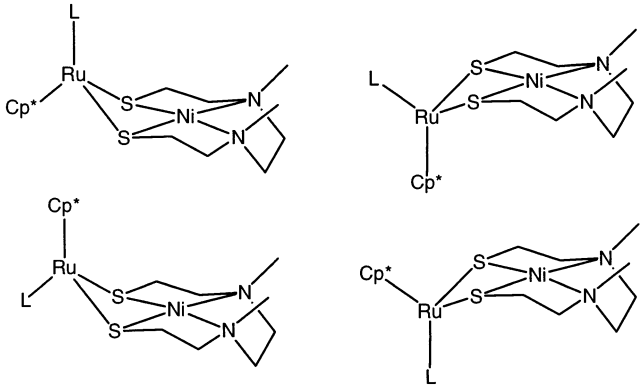

[a] The one in the upper left is observed.

diethyl-3,7-diazanonane-1,9-dithiolate) adopt similar conformations.[31,32] The NiS_2N_2 ligand adopts a bowl-like cavity under the η^2-O_2 ligand. In comparison to [**1**]$_2^{2+}$, the Ru(1)−S(1) and Ru(1)−S(2) distances of **2**$^+$ are 0.056−0.059 Å shorter. The O−O distance of 1.371(8) Å is similar to those observed in [Cp*Ru(dppe)(η^2-O_2)]$^+$ (1.398(5) Å)[33,34] and [Cp*Ru(dppm)(η^2-O_2)]$^+$ (1.37(1) Å),[34] although the Ru−O distances are slightly longer. The O_2 ligand was not displaced by CO and was also unreactive toward H_2 in refluxing MeCN solution.

Complex [**1**]$_2$(OTf)$_2$ also reacts with elemental sulfur at room temperature in MeCN solution to give the brown persulfide [Cp*Ru(NiS_2N_2)](η^2-S_2)]OTf, [**3**]OTf (eq 4).

$$[Cp^*Ru(NiS_2N_2)]_2^{2+} + 0.5\ S_8 \rightarrow \underset{[\mathbf{1}]_2^{2+}}{} \qquad 2\ \underset{\mathbf{3}^+}{[Cp^*Ru(NiS_2N_2)(S_2)]^+} \quad (4)$$

The ^{1}H NMR data for **3**$^+$ resemble that for the dioxygen complex **2**$^+$. Further supporting the structure proposed for **3**$^+$, the FAB-MS showed a parent ion for [Cp*Ru(NiS_2N_2)(S_2)]$^+$ (m/z = 565) and the fragment [Cp*Ru(NiS_2N_2)]$^+$ (m/z = 501).

Reactions of [1]$_2$(OTf)$_2$ with CO and MeNC. Acetonitrile solutions of [**1**]$_2$(OTf)$_2$ react with CO and MeNC to give the corresponding adducts [Cp*Ru(NiS_2N_2)L]OTf, [**4**]OTf for L = CO and [**5**]OTf for L = MeNC (eq 5).

$$[Cp^*Ru(NiS_2N_2)]_2^{2+} + 2\ L \rightarrow \underset{[\mathbf{1}]_2^{2+}}{} \qquad 2\ \underset{\mathbf{4}^+(L = CO)\ \ \mathbf{5}^+(L = CNMe)}{[Cp^*Ru(NiS_2N_2)(L)]^+} \quad (5)$$

The IR spectrum of **4**$^+$ exhibits ν_{CO} at 1901 cm^{-1}, the low value of which is indicative of the excellent electron-donating power of the NiS_2N_2 ligand. For comparison, ν_{CO} for the structurally related phosphine complexes [Cp*Ru(PMe_3)$_2$(CO)]$^+$ and [Cp*Ru(dppe)(CO)]$^+$ occur at 1935 and 1975 cm^{-1},[35,36] respectively. FAB-MS shows peaks for [Cp*Ru(NiS_2N_2)(CO)]$^+$ as well as [Cp*Ru(NiS_2N_2)]$^+$. The MeNC adduct [**5**]OTf proved to be spectroscopically similar to **4**$^+$, the ν_{CN} again occurring at relatively low energy at 2070 cm^{-1}. Addition of excess of MeNC with [**1**]$_2^{2+}$ gave the bis(adduct) [Cp*Ru(NiS_2N_2)(CNMe)$_2$]$^+$, which was characterized spectroscopically. Telling ^{1}H NMR data are the presence of diastereotopic CN*Me* signals as well as signals consistent with an unsymmetrically bound NiS_2N_2.

[Cp*Ru(Ni(bme*-daco))(MeCN)]OTf ([6]OTf). In this series of experiments we examined a bulkier version of the NiS_2N_2 species Ni(bme*-daco), where bme*-daco = [1,5-bis(2-mercapto-2-methylpropyl)-1,5-diazacyclooctane] (Chart 3). The goal was to generate a stable monomeric analogue of [**1**]$_2^{2+}$. Solutions of [Cp*Ru($NCMe)_3$]$^+$ and Ni(bme*-daco) react readily in MeCN solution to produce dark brown [Cp*Ru(NCMe)(Ni(bme*-daco))]$^+$ (**6**$^+$) (eq 6). FAB-MS analysis shows a

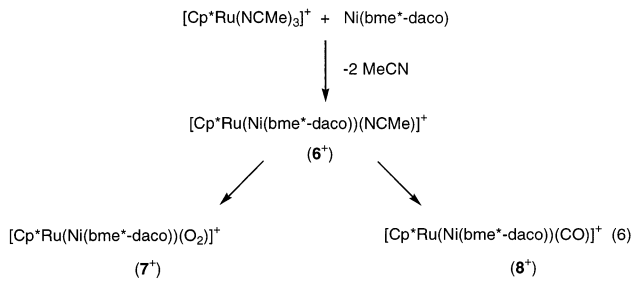

(32) Osterloh, F.; Saak, W.; Pohl, S. *Chem. Commun.* **1997**, 979−978.
(33) Kirchner, K.; Mauthner, K.; Mereiter, K.; Schmid, R. *J. Chem. Soc., Chem. Commun.* **1993**, 892−894.
(34) Jia, G.; Ng, W. S.; Chu, H. S.; Wong, W.-T.; Yu, N.-T.; Williams, I. D. *Organometallics* **1999**, *18*, 3597−3602.

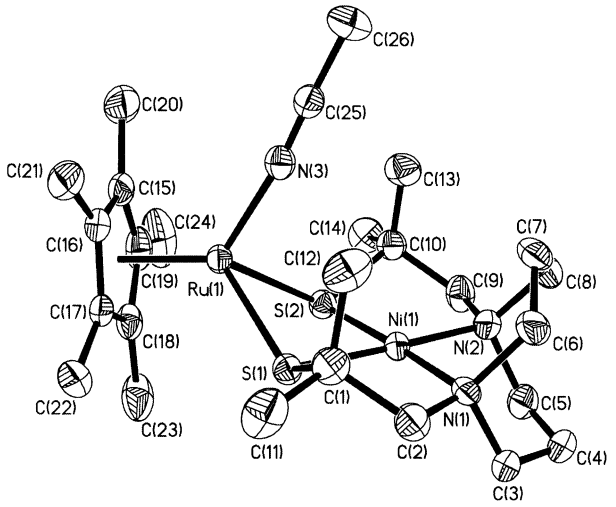

Figure 3. Molecular structure of the cation of [Cp*Ru(Ni(bme*-daco))(NCMe)]OTf, [**6**]OTf, with thermal ellipsoids drawn at the 50% probability level.

Table 3. Selected Bond Lengths (Å) and Angles (deg) for [6]OTf

Ru(1)−S(1)	2.4346(18)	N(3)−C(25)−C(26)	177.4(5)
Ru(1)−S(2)	2.4628(18)	C(25)−N(3)−Ru(1)	172.2(3)
Ru(1)−N(3)	2.051(4)	S(1)−Ni(1)−S(2)	85.39(8)
Ni(1)−S(1)	2.1519(17)	N(1)−Ni(1)−N(2)	92.79(16)
Ni(1)−S(2)	2.1548(17)	C(1)−S(1)−Ru(1)	123.80(15)
Ni(1)−N(1)	1.983(3)	C(1)−S(1)−Ni(1)	97.03(15)
Ni(1)−N(2)	1.977(4)	Ni(1)−S(1)−Ru(1)	93.75(8)
S(1)−Ru(1)−S(2)	73.21(6)	C(10)−S(2)−Ru(1)	125.37(14)
S(1)−Ru(1)−N(3)	99.04(11)	C(10)−S(2)−Ni(1)	97.22(15)
N(3)−Ru(1)−S(2)	96.84(11)	Ni(1)−S(2)−Ru(1)	92.89(7)

parent ion at $m/z = 585.1$ for $[Cp^*Ru(Ni(bme^*\text{-}daco))]^+$. The ^1H NMR spectrum of $\mathbf{6}^+$, while complex, exhibits signals that can be reasonably assigned to those expected for the bme*-daco ligand at δ 4.5−1.8. The geminal methyl groups appear as singlets at δ 1.57 and 1.13 and the Cp* methyl resonance is observed as a sharp singlet at δ 1.56. The coordinated MeCN rapidly exchanges in CD_3CN solution.

Crystallographic analysis demonstrates that $\mathbf{6}^+$, unlike $[\mathbf{1}]_2^{2+}$, consists of isolated Ru-Ni species wherein the thiolato ligands are only doubly bridging (Figure 3, Table 3). The Cp*Ru moiety adopts the usual piano-stool geometry as seen in $[\mathbf{1}]_2^{2+}$ and $\mathbf{2}^+$. The Ru centers feature an MeCN ligand with a Ru−N−C angle of 172.2(3)° and Ru(1)−N(3) distance of 2.051(4) Å. The Ni center sits in the pocket of the bme*-daco ligand in a square planar arrangement, as observed for the NiS_2N_2 ligands in the structures of $[\mathbf{1}]_2^{2+}$ and $\mathbf{2}^+$.

Complex $\mathbf{6}^+$ reacts rapidly with air in solution to give the peroxo complex $[Cp^*Ru(Ni(bme^*\text{-}daco))(\eta^2\text{-}O_2)]OTf$ ([**7**]OTf), which proved structurally similar to $\mathbf{2}^+$ (Supporting Information). Carbonylation of solutions of $\mathbf{6}^+$ gave the adduct $[Cp^*Ru(Ni(bme^*\text{-}daco))(CO)]OTf$, [**8**]OTf ($\nu_{CO} = 1914$ cm^{-1}).

$[CpRu(PPh_3)(NiS_2N_2)]Cl$. The phosphine ligands in $CpRu(PPh_3)_2Cl$ are known to be labile,[37] and this encouraged us to examine the reaction of (NiS_2N_2) and $CpRu(PPh_3)_2Cl$, a reaction that afforded the PPh_3 adduct $[CpRu(NiS_2N_2)(PPh_3)]Cl$ ([**9**]Cl), isolated as brick red crystals (eq 7).

$$CpRu(PPh_3)_2Cl + NiS_2N_2 \rightarrow [CpRu(NiS_2N_2)(PPh_3)]Cl + PPh_3 \quad (7)$$
$$[\mathbf{9}]Cl$$

Analysis by ^1H NMR spectroscopy and ESI-MS confirmed the formula. The PPh_3 ligand in $\mathbf{9}^+$ is not labile: complex $\mathbf{9}^+$ showed no reaction toward CO or $NaBH_4$. No reaction occurred between NiS_2N_2 and $CpRu(PPh_3)_2H$, indicating that the phosphine ligands in the hydrido complex are nonlabile (presumably due to the absence of π-donor ligands). We then examined the reaction of NiS_2N_2 with $CpRu(PPh_3)_2SH$, which is known to readily undergo CO-for-PPh_3 ligand exchange,[37] but this reaction instead afforded $Cp_4Ru_4S_4$, resulting from the thermally induced condensation of $CpRu(PPh_3)_2SH$.[38]

$[(arene)Ru(Cl)(NiS_2N_2)]PF_6$. Treatment of NiS_2N_2 with sources of $(arene)RuCl^+$ (arene = C_6Me_6, cymene) gave the expected adducts $[(arene)RuCl(NiS_2N_2)]^+$, isolated as their OTf^- salts (eq 8).

$$[(arene)RuCl_2]_2 + 2\ NiS_2N_2 \xrightarrow{2\ AgOTf} [(arene)RuCl(NiS_2N_2)]OTf \quad (8)$$
$$[\mathbf{10}]OTf\ (arene = cymene)$$
$$[\mathbf{11}]OTf\ (arene = C_6Me_6)$$

These cationic complexes proved thermally and chemically robust, and spectroscopic evidence supports the expected symmetric structures.

Summary

This project explored the preparative accessibility of thiolato-bridged Ni-Ru derivatives, as a starting point for the further development of functional models for bioorganometallic reaction centers. In particular the NiFe-hydrogenases and acetyl CoA synthase (ACS) both feature four-coordinate Ni centers bound to a second metal that is proposed to bind π-acids as either substrates (ACS) or constituative ligands. Although many derivatives of $Ni(SR)_2(amine)_2$ are known, the resulting bimetallic complexes studied to date are unreactive with respect to the binding of π-acid ligands.

On the basis of the present results, the NiS_2N_2 species could be expected to serve more generally as a supporting ligand in organometallic chemistry, e.g., in place of diphosphines. In terms of their affinity for (cyclopentadienyl)ruthenium(II) centers, the NiS_2N_2 species serve as innocent spectator ligands, although one that is more basic than typical Ph_2P-derived chelating diphosphines.[22] The high basicity of the NiS_2N_2 is further indicated by the tendency of $[Cp^*Ru(NiS_2N_2)]^+$ to dimerize via formation of μ_3-thiolato ligands.

The reactivity of $[Cp^*Ru(NiS_2N_2)]^+$ toward dioxygen differs from the corresponding oxygenations of NiS_2N_2 and Ni(bme*-daco), which afford sulfinato (RSO_2^-) and sulfenato (RSO^-) complexes.[39−42] It is well known that

(35) Tilley, T. D.; Grubbs, R. H.; Bercaw, J. E. *Organometallics* **1984**, *3*, 274.
(36) Xia, H. P.; Wu, W. F.; Ng, W. S.; Williams, I. D.; Jia, G. *Organometallics* **1997**, *16*, 2940−2947.
(37) Amarasekera, J.; Rauchfuss, T. B. *Inorg. Chem.* **1989**, *28*, 3875.
(38) Amarasekera, J.; Rauchfuss, T. B.; Wilson, S. R. *J. Chem. Soc., Chem. Commun.* **1989**, *14*, 14.
(39) Farmer, P. J.; Solouki, T.; Mills, D. K.; Soma, T.; Russell, D. H.; Reibenspies, J. H.; Darensbourg, M. Y. *J. Am. Chem. Soc.* **1992**, *114*, 4601−4605.

Table 4. Details of Data Collection and Structure Refinement for $[1]_2(OTf)_2$, [2]OTf, and [6]OTf

	$[\mathbf{1}]_2(OTf)_2$	[**2**]OTf	[**6**]OTf
chemical formula	$C_{19}H_{33}F_3N_2NiO_3RuS_3$	$C_{19}H_{33}F_3N_2NiO_5RuS_3$	$C_{27}H_{46}F_3N_3NiO_3RuS_3$
temp (K)	193(2)	193(2)	193(2)
cryst size (mm)	0.66 × 0.06 × 0.04	0.47 × 0.20 × 0.08	0.30 × 0.10 × 0.07
space group	$P\bar{1}$	$P2_1/c$	$P2_1/c$
a (Å)	9.252(2)	12.950(5)	11.084(10)
b (Å)	11.413(3)	15.019(5)	18.259(16)
c (Å)	13.835(3)	27.320(9)	16.519(15)
α (deg)	101.343(4)	90	90
β (deg)	99.102(4)	91.271(7)	92.401(8)
γ (deg)	101.017(4)	90	90
V (Å^3)	1376.5(6)	5312(3)	3340(5)
Z	2	8	4
D_{calcd} (Mg m^{-3})	1.569	1.707	1.252
μ (Mo Kα, mm^{-1})	0.71073	0.71073	0.71073
max./min. transmn	0.9950/0.8532	0.7744/0.6440	0.9890/0.8661
no. of reflns measd/indep	8562/5035	39985/12786	21653/7944
no. of data/restraints/params	5035/0/323	12786/1047/835	7944/0/380
GOF	0.896	0.968	0.939
R_{int}	0.0665	0.0671	0.0623
$R_1[I > 2\sigma]$ (all data)[a]	0.0491 (0.1047)	0.0588 (0.1513)	0.0456 (0.0964)
wR_2 $[I > 2\sigma]$ (all data)[b]	0.1032 (0.1197)	0.1547 (0.1919)	0.0943 (0.1079)
max. peak/hole (e$^-$/Å^3)	1.019/−0.691	1.340/−0.609	1.727/−1.202

[a] $R_1 = \sum||F_o| - |F_c||/\sum|F_o|$. [b] $wR_2 = \{\sum[w(F_o^2 - F_c^2)^2]/\sum[w(F_o^2)^2]\}^{1/2}$.

η^2-O_2 ligands are nucleophilic,[43,44] so it is not surprising that oxygen atom transfer from the peroxy ligand to the thiolate is not observed.

Experimental Section

General Considerations. All air-sensitive manipulations employed standard Schlenk line and drybox techniques. Solvents were dried using a solvent purification system similar to that described by Grubbs et al.[45] Published procedures were followed in the preparation of NiS_2N_2 ($S_2N_2^{2-}$ = SCH_2CH_2-$NMeCH_2CH_2NMeCH_2CH_2S$),[31] Ni(bme*-daco),[46] [Cp*Ru(NC-Me)$_3$]OTf,[47] $CpRu(PPh_3)_2Cl$,[48] and $[(arene)RuCl_2]_2$ (arene = cymene or C_6Me_6).[49] Elemental analyses were conducted by the Microanalytical Laboratory in the School of Chemical Sciences. ^{1}H NMR spectra were acquired on a Unity Varian 400 or a Unity Varian 500 NMR spectrometer. Infrared spectra were acquired on a Mattson Infinity Gold FT-IR spectrometer using solution cells with CaF_2 plates. Fast atom bombardment (FAB) and electrospray ionization-mass spectrometry (ESI-MS) were acquired using a Micromass 70 VSE double-focusing sector instrument and a Micromass Quattro QHQ quadrapole-hexapole-quadrapole instrument, respectively.

$[Cp^*Ru(NiS_2N_2)]_2(OTf)_2$ ($[\mathbf{1}]_2(OTf)_2$). A solution of 252 mg (0.495 mmol) of [Cp*Ru(NCMe)$_3$]OTf in 10 mL of MeCN was added to a solution of 134 mg (0.506 mmol) of NiS_2N_2 in 15 mL of MeCN. After 1 h, the resulting dark brown solution was reduced in volume to ca. 5 mL. The concentrate was layered with 15 mL of Et_2O and stored at −20 °C overnight. Dark brown crystals precipitated from solution and were collected and washed with Et_2O. Yield: 260 mg (81%). ^{1}H NMR (CD_3CN, 20.1 °C): *δ* 3.72 (br, m, 2H), 3.12 (br, m, 2H), 2.61 (m, 4H), 2.51 (s, 6H), 3.38 (br, m, 2H), 2.15 (m, 2H), 1.56 (br, s, 15H). ^{1}H NMR (CD_3CN, 60.1 °C): *δ* 3.72 (m, 2H), 3.13 (m, 2H), 2.65−2.57 (m, 4H), 2.51 (s, 6H), 2.39 (m, 2H), 2.18 (m, 2H), 1.61 (s, 15H). FAB-MS (MeCN): *m*/*z* 501 $[Cp^*Ru(NiS_2N_2)]^+$. Anal. Calcd for $C_{19}H_{33}F_3N_2NiO_3RuS_3$: C, 35.09; H, 5.11; N, 4.31. Found: C, 35.13; H, 5.22; N, 4.37.

$[Cp^*Ru(NiS_2N_2)(\eta^2\text{-}O_2)]$OTf ([2]OTf). A solution of 100 mg (0.077 mmol) of $[\mathbf{1}]_2(OTf)_2$ in 10 mL of MeCN was stirred in air for 1.5−2.0 h, resulting in a color change from dark brown to red-brown. The solvent volume was reduced under vacuum to ca. 2 mL and then layered with 15 mL of Et_2O, which was cooled to −20 °C for 8 h to produce red-brown crystals. Yield: 94 mg (95%). ^{1}H NMR (CD_3CN): *δ* 4.25 (m, 2H), 3.40 (m, 2H), 2.72 (m, 4H), 2.59 (s, 6H), 2.57 (m, 4H), 1.49 (s, 15H, Cp*). ESI-MS (MeCN): *m*/*z* 533 $[Cp^*Ru(NiS_2N_2)(\eta^2\text{-}O_2)]^+$. Anal. Calcd for $C_{19}H_{33}F_3N_2NiO_5RuS_3$: C, 33.44; H, 4.87; N, 4.10. Found: C, 33.80; H, 5.08; N, 4.29.

$[Cp^*Ru(NiS_2N_2)(\eta^2\text{-}S_2)]$OTf ([3]OTf). A solution of 142 mg (0.109 mmol) of $[\mathbf{1}]_2(OTf)_2$ and 10.0 mg (0.312 mmol) of S_8 was prepared in 15 mL of MeCN. After 2 h, the solvent volume was reduced to ca. 2 mL, and the concentrate was treated with 10 mL of Et_2O to give a brown precipitate of crude [**3**]OTf. Yield: 104 mg (74%). Dark brown single crystals were grown by diffusion of Et_2O into an MeCN solution of [**3**]OTf. ^{1}H NMR (CD_3CN): *δ* 4.09 (m, 2H), 3.30 (m, 2H), 2.62−2.49 (m, 6H), 2.52 (s, 6H), 2.39 (m, 2H), 1.41 (s, 15H). FAB-MS (MeCN): *m*/*z* 565 $[Cp^*Ru(NiS_2N_2)(S_2)]^+$; 501 $[Cp^*Ru(NiS_2N_2)]^+$. Anal. Calcd for $C_{19}H_{33}F_3N_2NiO_3RuS_5$: C, 31.94; H, 4.65; N, 3.92. Found: C, 32.03; H, 4.62; N, 4.11.

$[Cp^*Ru(NiS_2N_2)(CO)]$OTf ([4]OTf). A 15 mL solution containing 104 mg (0.080 mmol) of $[\mathbf{1}]_2(OTf)_2$ was purged with CO for 30 min, resulting in a color change from dark brown to deep red. The solvent volume was reduced to ca. 1 mL, and the concentrate was layered with 20 mL of Et_2O, which after 8 h produced red-brown crystals of [**4**]OTf at −20 °C. Yield: 80 mg (75%). ^{1}H NMR (CD_3CN): *δ* 4.00 (m, 2H), 3.43 (m, 2H), 2.80 (m, 4H), 2.62 (s, 6H), 2.58 (m, 2H), 2.18 (m, 2H), 1.75 (s, 15H). IR (MeCN): ν_{CO} 1901 cm^{-1}. FAB-MS (MeCN): *m*/*z* 529 $[Cp^*Ru(NiS_2N_2)(CO)]^+$; 501 $[Cp^*Ru(NiS_2N_2)]^+$. Anal. Calcd for $C_{20}H_{33}F_3N_2NiO_4RuS_3$: C, 35.41, H, 4.90, N, 4.13. Found: C, 35.66, H, 5.03, N, 4.27.

$[Cp^*Ru(NiS_2N_2)(CNMe)]$OTf ([5]OTf). To a solution of 86.0 mg (0.066 mmol) of $[\mathbf{1}]_2(OTf)_2$ in 10 mL of MeCN was

(40) Farmer, P. J.; Solouki, T.; Soma, T.; Russell, D. H.; Darensbourg, M. Y. *Inorg. Chem.* **1993**, *32*, 4171−4172.
(41) Farmer, P. J.; Verpeaux, J.-N.; Amatore, C.; Darensbourg, M. Y.; Musie, G. *J. Am. Chem. Soc.* **1994**, *116*, 9355−9356.
(42) Font, I.; Buonomo, R.; Reibenspies, J. H.; Darensbourg, M. Y. *Inorg. Chem.* **1993**, *32*, 5897−5898.
(43) Gubelmann, M. H.; Williams, A. F. *Struct. Bonding* **1983**, *55*, 1−65.
(44) Beaulieu, W. B.; Mercer, G. D.; Roundhill, D. M. *J. Am. Chem. Soc.* **1978**, *100*, 1147−1152.
(45) Pangborn, A. B.; Giardello, M. A.; Grubbs, R. H.; Rosen, R. K.; Timmers, F. J. *Organometallics* **1996**, *15*, 1518−1520.
(46) Darensbourg, M. Y.; Font, I.; Pala, M.; Reibenspies, J. H. *J. Coord. Chem.* **1994**, *32*, 39−49.
(47) Fagan, P. J.; Ward, M. J.; Calabrese, J. C. *J. Am. Chem. Soc.* **1989**, *111*, 1698−1719.
(48) Bruce, M. I.; Windsor, N. J. *Aust. J. Chem.* **1977**, *30*, 1601−1604.
(49) Bennett, M. A.; Huang, T.-N.; Matheson, T. W.; Smith, A. K. *Inorg. Synth.* **1982**, *21*, 74−78.

added 0.20 mL (0.18 mmol) of a 0.91 M stock solution of CNMe in MeCN. The solution initially became red for 2 min and then turned red-brown. After stirring for 2 h, the solvent volume was reduced to ca. 1 mL, and the solution was then layered with 10 mL of Et_2O to produce brown crystals. Yield: 55 mg (60%). ^{1}H NMR (CD_3CN): δ 4.00 (2H, m), 3.87 (3H, s), 3.27 (2H, m), 2.64 (4H, m), 2.54 (6H, s), 2.44 (2H, m), 1.87 (2H, m), 1.67 (15H, s). IR (KBr): ν_{CN} 2070 cm^{-1}. FAB-MS (MeCN): *m*/*z* 542.0 [Cp*Ru(NiS_2N_2)(CNMe)]$^+$, 501.0 [Cp*Ru(NiS_2N_2)]$^+$. Anal. Calcd for $C_{21}H_{36}F_3N_3NiO_3RuS_3$: C, 36.48; H, 5.25; N, 6.08. Found: C, 37.02; H, 5.54; N, 6.14.

[Cp*Ru(NiS_2N_2)($CNMe)_2$]OTf. To a solution of 100 mg (0.077 mmol) of [**1**]$_2$(OTf)$_2$ in 10 mL of MeCN was added 1.00 mL (0.46 mmol) of a 0.46 M solution of CNMe in MeCN. The solution was stirred for 6 h and during this time became red. The volume was then reduced and 15 mL of Et_2O was added. A red crystalline solid was produced after 1 day at −20 °C, collected by filtration, and dried in vacuo. Yield: 99.0 mg (88%). ^{1}H NMR (CD_3CN): 3.74 (s, 3H, Me), 3.45 (s, 3H, Me), 3.21(m, 2H), 3.04 (m, 1H), 2.98 (m, 1H), 2.96 (s, 3H, Me), 2.82 (s, 3H, Me), 2.64 (m, 1H), 2.58 (m, 1H), 2.49−2.36 (m, 4H), 2.19 (m, 1H), 2.09 (m, 1H), 1.73 (s, 15H, Cp*). IR (MeCN): ν_{CN} 2159; 2125 cm^{-1}. FAB-MS (MeCN): *m*/*z* 583.1 [Cp*Ru(NiS_2N_2)-($CNMe)_2$]$^+$; 501.1 [Cp*Ru(NiS_2N_2)]$^+$.

[Cp*Ru(Ni(bme*-daco))(NCMe)]OTf ([6]OTf). In a glovebox, a solution of 27.0 mg (0.053 mmol) of [Cp*Ru($NCMe)_3$]-OTf in 2 mL of MeCN was added to a solution of 19.0 mg (0.055 mmol) of Ni(bme*-daco) in 3 mL of MeCN. The dark solution was stirred for 2 h followed by reduction of the solvent volume to ca.1 mL. Layering with 6 mL of Et_2O afforded red-brown crystals of [**6**]OTf. Yield: 40 mg (98%). ^{1}H NMR (CD_3CN): δ 4.53 (m, 1H), 3.59 (dt, 2H), 2.92 (m, 2H), 2.61 (dt, 2H), 2.54−2.44 (m, 6H), 1.83 (m, 3H), 1.57 (s, 6H, 2 Me), 1.56 (s, 15H, C_5Me_5), 1.13 (s, 6H, 2 Me). FAB-MS (CH_3CN): *m*/*z* 585.1 [Cp*RuNi(bme*-daco)]$^+$. Anal. Calcd for $C_{27}H_{46}F_3N_3NiO_3$-RuS_3: C, 41.92; H, 5.99; N, 5.43. Found: C, 41.35; H, 5.90; N, 5.28.

[Cp*Ru(Ni(bme*-daco))(η^2-O_2)]OTf ([7]OTf). A 5 mL solution of 20 mg (0.029 mmol) of [**6**]OTf in MeCN was stirred in air for 30 min. The solvent was then removed under vacuum, producing a red-brown solid, which was recrystallized from a 10:1 mL mixture of MeCN/Et_2O at −20 °C overnight. Yield: 18 mg (80%). ^{1}H NMR (CD_3CN): δ 3.82 (m, 1H), 3.54 (m, 2H), 3.18 (m, 2H), 2.78 (m, 4H), 2.66−2.42 (m, 6H), 1.88, (m, 1H), 1.73 (s, 6H, 2 Me), 1.43 (s, 15 H, Cp*), 1.37 (s, 6H, 2 Me). An analytically pure sample of this compound was not obtained.

[Cp*Ru(Ni(bme*-daco))(CO)]OTf ([8]OTf). A 5 mm NMR tube charged with a 1 mL of CD_3CN solution containing 10.0 mg (0.013 mmol) of [**6**]OTf was purged with CO for 1 h, during which time the dark solution became red. ^{1}H NMR (CD_3CN): δ 4.44 (m, 1H), 3.60 (m, 2H), 2.94 (m, 2H), 2.68−2.51 (m, 8H), 2.06−1.85 (m, 3H), 1.75 (s, 15H, Cp*), 1.65 (s, 6H, 2 Me), 1.13 (s, 6H, 2 Me). IR (CD_3CN): ν_{CO} = 1914 cm^{-1}. Anal. Calcd for $C_{26}H_{43}F_3N_2NiO_4RuS_3$: C, 40.95; H, 5.95; N, 3.67. Found: C, 40.18; H, 5.64; N, 3.98.

[CpRu(NiS_2N_2)(PPh_3)]Cl ([9]Cl). A solution of 100 mg (0.138 mmol) of CpRu($PPh_3)_2$Cl and 37.0 mg (0.140 mmol) of NiS_2N_2 in 15 mL of MeCN was heated at reflux for 12 h. After removal of the solvent, the red residue was washed with 30 mL of Et_2O. Brick red crystals were grown after 48 h by slow diffusion of Et_2O into a solution of [**9**]Cl in 4 mL of MeCN at room temperature. Yield: 70 mg (69%). ^{1}H NMR (CD_3CN): δ 7.43−7.26 (15H, m, Ph), 4.51 (5H, s, C_5H_5), 4.04 (2H, m), 3.89 (2H, m), 3.62 (2H, m), 3.42 (2H, m), 3.28 (2H, m), 2.83 (6H, s, 2 Me), 2.69 (2H, m). ^{31}P NMR: δ 52.6. FAB-MS (MeCN): *m*/*z* 693.0 [CpRu(NiS_2N_2)(PPh_3)]$^+$, 430.9 [CpRu(NiS_2N_2)]$^+$. Anal. Calcd for $C_{31}H_{38}ClN_2NiRuPS_3$: C, 51.08; H, 5.25; N, 3.84. Found: C, 49.99; H, 5.55; N, 3.88.

[(cymene)RuCl(NiS_2N_2)]OTf ([10]OTf). A 5 mL MeCN solution of 29.0 mg (0.11 mmol) of AgOTf was added dropwise to a solution of 34 mg (0.06 mmol) of [(cymene)$RuCl_2]_2$ in 5 mL of MeCN. The solution became light yellow with a white precipitate and was stirred for another 20 min, then allowed to settle. The yellow solution was filtered and transferred to a 10 mL solution of 30 mg (0.11 mmol) of NiS_2N_2 in MeCN. The brown solution became cherry-red immediately upon the addition. After 2 h, the solution was reduced in volume to ca. 1 mL, layered with 10 mL of Et_2O, and stored at −20 °C overnight to afford a red powder. Yield: 57 mg (80%). ^{1}H NMR ($CDCl_3$): δ 5.45 (2H, d, J = 6.0 Hz), 5.31 (2H, d, J = 6.0 Hz), 4.70 (2H, m), 3.84 (2H, m), 3.61−3.44 (6H, m), 3.06 (6H, s, 2 N-Me), 2.94 (2H, m), 2.81 (1H, septet, J = 6.8 Hz), 2.15 (3H, s, Me), 1.20 (6H, d, J = 6.8 Hz, 2 Me). FAB-MS (MeCN): *m*/*z* 535.0 [($C_{10}H_{14}$)Ru(NiS_2N_2)Cl]$^+$. Anal. Calcd for $C_{19}H_{32}ClF_3N_2$-NiO_3RuS_3: C, 33.32; H, 4.71; N, 4.09. Found: C, 33.44; H, 5.08; N, 4.19.

[(C_6Me_6)Ru(NiS_2N_2)Cl]OTf ([11]OTf). Complex [**11**]OTf was prepared in a manner similar to [**10**]OTf by reacting 100 mg (0.15 mmol) of [(C_6Me_6)$RuCl_2]_2$ in 5 mL of MeCN and 77 mg (0.30 mmol) of AgOTf in 5 mL of MeCN. The resulting slurry was filtered into a solution of 79.0 mg (0.30 mmol) of NiS_2N_2 in 10 mL of MeCN. After 2 h, the solvent was reduced in vacuo to ca. 1 mL and layered with Et_2O. After 1 day, a red powder precipitated. Yield: 58 mg (70%). ^{1}H NMR (CD_3CN): δ 4.40 (m, 2H), 3.23 (m, 2H), 2.73 (m, 2H), 2.57 (s, 6H), 2.53 (m, 2H), 2.42−2.30 (m, 4H), 1.98 (s, 18H, C_6Me_6). FAB-MS (MeCN): *m*/*z* 563.0 [(C_6Me_6)Ru(NiS_2N_2)Cl]$^+$. Anal. Calcd for $C_{21}H_{36}ClF_3N_2NiO_3RuS_3$: C, 35.38; H, 5.09; N, 3.93. Found: C, 35.30; H, 5.17; N, 4.18.

Crystallography. Crystals were mounted on thin glass fibers using oil (Paratone-N, Exxon). Data were collected at 193(2) K on a Siemens CCD diffractometer. Crystal and refinement details are given in Table 4. All structures were solved using SHELXTL and direct methods; correct atomic positions were deduced from an *E* map or by an unweighted difference Fourier synthesis. H atom *U*'s were assigned as 1.2 times the U_{eq}'s of adjacent C atoms. Non-H atoms were refined with anisotropic thermal coefficients. Successful convergence of the full-matrix least-squares refinement of F^2 was indicated by the maximum shift/error for the last cycle.

Acknowledgment. This research was supported by NIH.

Supporting Information Available: Atomic coordinates, bond lengths and angles, anisotropic displacement parameters, and hydrogen coordinates for [**1**]$_2$(OTf), [**2**]OTf, [**6**]OTf, and [**7**]OTf. Variable-temperature ^{1}H NMR spectrum of [**1**]$_2^{2+}$. A molecular structure of [**7**]OTf is included with thermal ellipsoids drawn at the 30% probability level. This material is available free of charge via the Internet at http://pubs.acs.org.

OM020724E